

T-Stress solutions for a semi-elliptical axial surface crack in a cylinder subjected to mode-I non-uniform stress distributions

メタデータ	言語: English 出版者: 公開日: 2010-09-07 キーワード (Ja): キーワード (En): 作成者: <input checked="" type="checkbox"/> MESHII, <input checked="" type="checkbox"/> Toshiyuki, TANAKA, Tomohiro, LU, Kai メールアドレス: 所属:
URL	http://hdl.handle.net/10098/2460

T-stress Solutions for a Semi-Elliptical Axial Surface Crack in a Cylinder

Subjected to Mode-I Non-Uniform Stress Distributions

Toshiyuki MESHII ^{a*}, Tomohiro TANAKA ^b and Kai LU ^b

^a Graduate School of Engineering, University of Fukui, 3-9-1 Bunkyo, Fukui, Fukui, JAPAN.

^b Graduate Student, University of Fukui, 3-9-1 Bunkyo, Fukui, Fukui, JAPAN.

*Correspondent, E-mail : meshii@u-fukui.ac.jp, FAX : +81-776-27-9764

Abstract

This paper presents the *T*-stress solutions (T_{11} and T_{33}) for semi-elliptical axial surface cracks in a cylinder subjected to mode-I non-uniform stress on the crack surface. Two cylindrical geometries with inner radius (R_i) to wall thickness (t) ratios $R_i/t = 5$ and 10 were considered. The *T*-stresses were applied along the crack front for normalized crack depth values a/t of 0.2 , 0.4 and 0.5 and aspect ratios a/c of 0.2 , 0.4 , 0.6 and 1.0 . Three stress distribution; uniform, linear and parabolic were applied to the crack face. In addition to these solutions, concrete formulation of the superposition principle is given for the T_{33} -stress, which is known as an elastic parameter that describes the out-of-plane crack tip constraint effect. Then, the validity of the formulation was shown through application of our *T*-stress solutions to the problem of an axial semi-elliptical surface crack in a cylinder subjected to internal pressure, and checking that the principle of superposition holds for the problem.

Key words: Fracture mechanics, Finite element analysis, Elastic *T*-stress, Superposition principle,

Constraint effect, Surface crack, Non-uniform stress distribution, Internal pressure, Cylinder.

Nomenclature

a : depth of a semi-elliptical crack

c : length of a semi-elliptical crack

p : internal pressure

t : cylinder wall thickness

r and θ : in-plane polar coordinates of the plane normal to the crack front (Fig. 1)

u : local coordinate along crack depth (Figs. 2 and 3)

x_j : crack tip local coordinates ($j = 1\sim 3$, see Fig. 1)

z : local coordinate normal to crack depth (Fig. 3)

E : Young's modulus

K_I : local mode I stress intensity factor

L : cylinder length

L_{Box} : mesh generation parameter (Fig. 5)

Q : load system

R , Z and Θ : cylindrical coordinates (Fig. 2)

R_i and R_o : inner and outer radius of a cylinder

R_s : mesh generation parameter (Fig. 5)

T_{11} and T_{33} : T-stresses (Eq. (1))

V_{11} and V_{33} : normalized T-stresses (Eq. (7))

Δ : Difference in T-stresses solutions by direct calculation and by superposition (Tables 8~11)

Δl , Δl_j ($j = 1\sim 4$): mesh generation parameter (Fig. 5)

ϕ : angle to specify location on the semi-elliptical crack front (Figs. 2 and 4)

$\kappa = R_o / R_i$

ν : Poisson's ratio

$\rho = R / R_i$

1. Introduction

The limited ability of a single parameter such as the stress intensity factor (SIF) K or J-Integral J to fully characterize crack tip conditions irrespective of geometry and load level has been recognized for years [1, 2]. To overcome this problem, two parameter description of the crack-tip stress-strain state have been studied over the past two decades. The so-called elastic T -stress, or the second term of the Williams [3] series expansion for linear elastic crack tip fields, have been strong candidates as the second parameter of this two-parameter approach. Larsson and Carlsson [2] and Rice [4] showed that the sign and magnitude of the T -stress substantially changed the size and shape of the plane strain crack tip plastic zone at finite load levels. Bilby et al. [5] showed that the T -stress has a strong influence on the magnitude of hydrostatic triaxiality in the near crack tip elastic–plastic fields. The important features emerging from these works are that: 1) the sign and magnitude of T -stress can substantially alter the level of crack tip stress triaxiality, hence influence crack tip constraint, and 2) positive T -stress strengthens the level of crack tip stress triaxiality and leads to high crack tip constraint; while negative T -stress reduces the level of crack tip stress triaxiality and leads to the loss the crack tip constraint. Though the T -stress is an elastic parameter, the later works by Al-Ani and Hancock [6], Betegon and Hancock [7], Du and Hancock [8] and O’Dowd and Shih [9] indicated that the T -stress, in addition to the J , provides a practical two-parameter characterization of plane strain elastic–plastic crack tip fields (corresponding to, for example, materials in the lower to mid-transition temperature range; referred to as “cleavage after

significant plastic deformation, but before the initiation of ductile growth” by some researchers [10]) in a variety of crack configurations and loading conditions. These works were focused on 2D (in-plane) crack tip constraint issues, and thus, the methodology was effective in regard to explaining the effect of crack depth on the fracture toughness testing [10]. Hereafter, in-plane T -stress will be denoted as T_{11} (Fig. 1).

On the other hand, out-of-plane crack tip constraint is also known to have a significant influence on the fracture behavior of materials [11], and work have been done to express this constraint along the 3D crack front by the out-of-plane T -stress T_{33} . Using an analytical technique, Gao [12] analyzed the variation of T_{11} and T_{33} along a slightly wavy 3D crack front. Numerical techniques based on 3D finite elements for calculating the distribution of these T -stresses along a curved 3D crack front were developed by Nakamura and Parks [13]. Using their numerical method, Wang and co-workers evaluated the T -stresses solutions for a semi-elliptical surface crack fronts in a finite thickness plate under various loading conditions [14, 15], and a quarter-elliptical corner crack in a finite thickness plate subjected to tension and bending [16].

In order to apply the two parameter fracture mechanics methodology, it is important to provide T -stresses solutions for various crack configurations under various load conditions. So in this paper, concrete formulation of the superposition principle is given for the T_{33} -stress. Then, the T -stress solutions (T_{11} and T_{33}) are presented for a semi-elliptical axial surface crack in a cylinder subjected to mode-I non-uniform stress on the crack face (Fig. 2). Two cylindrical geometries with inner radius of the cylinder

(R_i) to wall thickness (t) ratios $R_i/t = 5$ and 10 were considered. The T -stresses were presented along the crack front for normalized crack depth values a/t of 0.2 , 0.4 and 0.5 and normalized crack length values a/c of 0.2 , 0.4 , 0.6 and 1.0 . Three stress distributions: uniform, linear and parabolic were applied to the crack face. Finally, the validity of these solutions was shown by applying our T -stress solutions to the problem of an axial semi-elliptical surface crack in a cylinder subjected to internal pressure, and checking that the principle of superposition holds for the problem.

2. Principle of superposition for T_{33}

In this section, the superposition method for the T -stresses calculation is discussed first. Then the concrete formula based on this method used to obtain T_{33} -stress solutions for other stress distributions is deduced. The concrete formula for T_{11} -stress worked out by Wang et al. [15] is also introduced for reference.

In an isotropic linear elastic body containing a crack subjected to symmetric (mode I) loading, the leading terms (up to order $O(1)$) in a series expansion of the stress field very near the crack front are [13]

$$\begin{Bmatrix} \sigma_{11} \\ \sigma_{22} \\ \sigma_{33} \\ \tau_{12} \\ \tau_{23} \\ \tau_{31} \end{Bmatrix} = \frac{K_I}{\sqrt{2\pi r}} \begin{Bmatrix} \cos \frac{\theta}{2} \left(1 - \sin \frac{\theta}{2} \sin \frac{3\theta}{2} \right) \\ \cos \frac{\theta}{2} \left(1 + \sin \frac{\theta}{2} \sin \frac{3\theta}{2} \right) \\ 2\nu \cos \frac{\theta}{2} \\ \sin \frac{\theta}{2} \cos \frac{\theta}{2} \cos \frac{3\theta}{2} \\ 0 \\ 0 \end{Bmatrix} + \begin{Bmatrix} T_{11} \\ 0 \\ T_{33} \\ 0 \\ 0 \\ 0 \end{Bmatrix} \quad (1)$$

$$T_{33} = E\varepsilon_{33} + \nu T_{11} \quad (2)$$

where r and θ are the in-plane polar coordinates of the plane normal to the crack front shown in Fig. 1 and K_I is the local mode I stress intensity factor. Here x_1 is the direction formed by the intersection of the plane normal to the crack front and the plane tangential to the crack plane. The terms T_{11} and T_{33} are the amplitudes of the second orders term in the three-dimensional series expansion of the crack front stress field in the x_1 and x_3 directions, respectively.

First, consider a cracked two dimensional specimen loaded by mode I load system Q , as demonstrated in Fig. 3. The stress field of this problem can be divided into two parts: the regular field which appears under the same loading conditions in the uncracked specimen (problem Fig. 3(b)), and a corrective field due to the presence of the crack (Fig. 3 (c)). Note that the corrective field (Fig. 3(c)) is generated by the crack face pressure, $\sigma_z(u/a)$, induced by the load system Q in the uncracked body. Therefore, the elastic SIF or T-stresses for the problem (Fig. 3 (a)) can be calculated from the summation of the SIF or T -stresses for these two problems, respectively;

$$\begin{aligned} K &= K_{\text{uncrack}} + K_{\text{surface}} \\ T_{11} &= T_{11\text{uncrack}} + T_{11\text{surface}} \\ T_{33} &= T_{33\text{uncrack}} + T_{33\text{surface}} \end{aligned} \quad (3)$$

where subscripts uncrack and surface show that the parameters corresponds to an uncracked problem (Fig. 3 (b)) and to a cracked problem (Fig. 3 (c)), respectively.

In Eq. (3), $K_{\text{uncrack}} = 0$ is well known, but T -stresses for the uncracked body is not zero. Wang [15] formulated $T_{11 \text{ uncrack}}$ at crack tip A as follows.

$$T_{1\text{uncrack}} = \lim_{r \rightarrow +0} \{ \sigma_{11}|_{\theta=0} - \sigma_{22}|_{\theta=0} \} = (\sigma_{11} - \sigma_{22})|_A \quad (4)$$

In the following, we formulated the superposition principle for T_{33} stress. Initially the uncracked problem in Fig. 3 (b) is considered as a state of closed crack, due to applying stress $\{-\sigma_z(u/a)\}$ on the crack surface. With this approach the stress distribution near point A in Fig. 3 (b) can be formally described by Eq. (1). By considering the $\theta = 0$ plane, and by subtracting the singular term in σ_{33} and σ_{22} in Eq. (3), $T_{33\text{uncrack}}$, or the stress at point A ($r \rightarrow +0$) is deduced as follows.

$$T_{33\text{uncrack}} = \lim_{r \rightarrow +0} \{ \sigma_{33}|_{\theta=0} - 2\nu\sigma_{22}|_{\theta=0} \} = (\sigma_{33} - 2\nu\sigma_{22})|_A \quad (5)$$

The validity of Eq. (5) will be shown in section 3 for a the problem of an axial semi-elliptical surface crack in a cylinder subjected to internal pressure.

3. Finite element analysis for a semi-elliptical axial surface crack in a cylinder subjected to mode-I non-uniform stress distributions

3.1. Method of T -stresses extractions and numerical examples

T_{11} was obtained by using the domain integral and interaction integral techniques [13], which is a ready to use function in WARP3D [17]. These techniques have been widely used in the past for calculating various T_{11} solutions [15, 16, 18, 19]. Finally, T_{33} was evaluated from Eq. (2).

To show the validity of our mesh generation and T -stresses extraction process, we considered the case

of a quarter-elliptical corner crack subjected to tension σ_0 (Fig. 4 left), for which T_{11} and T_{33} solutions are known [16]. The case of $a/t = 0.2$, $a/c = 0.4$, $W/c = 32$, $L/W = 1$ was considered. The finite element analyses were made with 20-noded isoparametric three-dimensional solid elements using WARP3D [17].

In order to model the square root singularity at the crack tip, three dimensional prism elements with four mid-side nodes at the quarter points (singular element: a degenerate cube with one face collapsed) were used and the separate crack tip nodal points were constrained to have the same displacement [20]. Eight singular elements were used around the crack tip, which is common for all cases in this work. Material constants for Young's modulus $E = 206$ GPa and Poisson's ratio $\nu = 0.3$ were applied. Considering the symmetry condition, one half of the structure was modeled as shown in Fig. 4 right. In this model, K and T -stresses convergence was checked by making parameter studies of the singular element size in the radial direction Δl and along the crack front Δc , under the condition that the spider web radius $R_s = 20 \Delta l$ (Fig. 5). The selected crack tip element size was $\Delta l/a = 0.01$, $\Delta c_a/\Delta l = 17.3$ and $\Delta c_c/\Delta l = 6.6$. The results are summarized in Table 1 in the form of $V_{kk} = T_{kk}/\sigma_0$. Since it is known that the values of the T -stresses at or in the vicinity of the free surfaces ($\phi = 0$) were found to be unreliable [13], T -stresses for $\phi/(\pi/2) = 1/4$, $1/2$, $3/4$ and 1 were considered. We see from Table 1 that our T -stresses are in good agreement with the reference values. Though only one result is presented in this paper, similar results were obtained for other crack configurations. Thus, we consider that the mesh generation procedure together with the T -stresses extraction procedure was validated.

3.2. *T*-stresses for a semi-elliptical axial surface crack in a cylinder subjected to mode-I non-uniform stress distributions

Three-dimensional finite elements were used to model the symmetric quarter of a cylinder containing an inner surface semi-elliptical crack. Figure 2 shows the geometry and co-ordinate system used. The finite element analyses were made with 20-noded isoparametric three-dimensional solid elements using WARP3D [17]. Eight singular elements were always used around the crack tip, which is common for all cases in this work. Aspect ratios a/c of 0.2, 0.4, 0.6 and 1.0 with normalized crack depth of $a/t = 0.2, 0.4$ and 0.5 were considered. Three stress distributions: uniform, linear and parabolic (i.e., $j = 0, 1$ and 2 in Eqs (6) and (7)) were applied to the crack face.

$$\sigma_{\Theta}(u/a) = \sum_{j=0}^2 \sigma_j \cdot (u/a)^j \quad (6)$$

$$T_{kk \text{ surface}} = \sum_{j=0}^2 \sigma_j \cdot V_{kkj} \quad (k = 1 \text{ or } 3) \quad (7)$$

Here, $u = R - R_i$, with R and R_i radius and inner radius, respectively. In all analyses in the current calculations, wall thickness $t = 10$ mm, cylinder length to wall thickness ratio $L/t = 20$, Young's modulus $E = 206$ GPa and Poisson's ratio of $\nu = 0.3$ were applied. A typical finite element mesh is illustrated in Fig. 6. In these models, K and T -stresses convergence was checked by making parameter studies of the singular element size in the radial direction Δl and along the crack front Δc . The selected crack tip element size is summarized in Table 2.

Since it is known that the values of the T -stresses at or in the vicinity of the free surfaces ($\phi = 0$) were

found to be unreliable [13], T -stresses for $\phi / (\pi/2) = 1/4, 1/2, 3/4$ and 1 were considered in the present work. Normalized T_{11} and T_{33} solutions along the crack front for an axial semi-elliptical surface crack in a cylinder subjected to mode-I non-uniform stress distribution are summarized in Tables 3~6, in the form of V_{11} and V_{33} , as defined in Eq. (7).

Next, we validated our T -stress solutions in these tables by applying the superposition principle to these solutions to the axial semi-elliptical surface crack in a cylinder subjected to internal pressure. In concrete, T -stresses obtained from Tables 3~6 and Eqs. (3)~(5), were compared with those directly extracted from FEA under internal pressure loading. This validation of our T_{33} solution is also expected to provide the evidence that our superposition formulation of T_{33} has sufficient accuracy.

To apply superposition principle Eq. (3), $T_{kk \text{ surface}}$ and $T_{kk \text{ uncrack}}$ (where, $k = 1$ or 3) are necessary.

$T_{kk \text{ surface}}$ under the polynomial stress distribution in Eq. (6) is obtained from Eq. (7), using the coefficients V_{kkj} (tabulated in Tables 3~6) once the coefficients σ_j s are known. Since one of the purposes of this study was first to validate the superposition principle, inner pressure $p = 1$ MPa was applied on the inner surface of the cylinder, but not on the crack faces. The ends of the cylinder were set as thrust free. For this case, the analytical stresses for an uncracked cylinder are given as [21],

$$\begin{aligned}\sigma_R(\rho = R/R_i) &= -\frac{(\kappa/\rho)^2 - 1}{\kappa^2 - 1} p \\ \sigma_\Theta(\rho = R/R_i) &= \frac{(\kappa/\rho)^2 + 1}{\kappa^2 - 1} p \\ \sigma_Z(\rho = R/R_i) &= 0\end{aligned}\quad (8)$$

where σ_R and σ_Θ are radial and circumferential stress at radius R , and κ is outer to inner radius ratio R_o/R_i .

It is clear from Eq. (8) that the crack opening stress $\sigma_{22} = \sigma_{\Theta}$ varies according to R^{-2} , and thus, the stress distribution in the range of $0 \leq u/a \leq 1$ cannot be generally expressed in the form of Eq. (6). However, for the cases we considered, σ_{Θ} can be approximated as a quadratic (almost linear) function of u/a as follows,

$$\sigma_{\Theta}(u/a)/p = \sum_{j=0}^2 \frac{\sigma_j}{p} \left(\frac{u}{a}\right)^j \quad (9)$$

and thus, the $T_{kk \text{ surface}}$ ($k = 1$ or 3) for this problem is given by Eq. (7). σ_j/p for the cases considered here are given in Table 7.

To obtain the $T_{kk \text{ uncrack}}$ with Eq. (4) and (5), σ_{11} , σ_{33} and $\sigma_{22} = \sigma_{\Theta}$ at crack tip location A in Fig. 2 are necessary. These stresses vary with the location A, and are given as follows.

$$\begin{aligned} \sigma_{11}(\phi) &= -\sigma_R \left((R_i + a \sin \phi) / R_i \right) \cdot \left\{ \sin(\tan^{-1}(\frac{c}{a} \tan \phi)) \right\}^2 \\ \sigma_{22}(\phi) &= \sigma_{\Theta} \left((R_i + a \sin \phi) / R_i \right) \\ \sigma_{33}(\phi) &= -\sigma_R \left((R_i + a \sin \phi) / R_i \right) \cdot \left\{ \cos(\tan^{-1}(\frac{c}{a} \tan \phi)) \right\}^2 \end{aligned} \quad (10)$$

Substituting back to Eqs. (4) and (5), T_{33} obtained by applying the superposition principle, labeled as $T_{33 \text{ sup}}$, is given for this problem as

$$\begin{aligned} T_{11 \text{ sup}}(\phi) &= \{ \sigma_{11}(\phi) - \sigma_{22}(\phi) \} + \sum_{j=0}^2 \sigma_j \left(\frac{u}{a}\right) \cdot V_{11j} \\ T_{33 \text{ sup}}(\phi) &= \{ \sigma_{33}(\phi) - 2\nu \sigma_{22}(\phi) \} + \sum_{j=0}^2 \sigma_j \left(\frac{u}{a}\right) \cdot V_{33j} \end{aligned} \quad (11)$$

where V_{kkj} is given in Tables 3 ~6. The normalized $T_{11 \text{ sup}}$ (for concrete, $T_{11 \text{ sup}}/p$) was compared with the direct solution T_{11}/p in Tables 8 and 9. $T_{33 \text{ sup}}/p$ was compared with the direct solution T_{33}/p in Tables 10 and 11.

Data from Tables 8~9 shows that the difference between both solutions is less than 0.15% for T_{11} at

the four crack tip locations ϕ . The difference in the case for T_{33} was larger than T_{11} , but less than 0.93%. Though only one superposition example is presented in this paper, the validity of Eq. (5) has been confirmed for other cracked structures, such as quarter-elliptical corner surface crack in a plate, and thus, it is clear that T_{33} can be obtained by the concrete superposition formulation Eqs. (3) and (5) with sufficient accuracy.

4. Discussions

In Tables 8~11, T -stresses solutions for an axial semi-elliptical surface crack in a cylinder subjected to internal pressure were presented. Referring to these tables, the T_{11} and T_{33} for all cases (crack and cylinder configuration) are negative. This tendency is preferable, because a decrease in crack tip constraint can be expected for negative T -stresses [5]. However, it must be remembered that our study was focused on validating the superposition principle, and thus, internal pressure was not applied at the crack surfaces. At the least, this internal pressure will surely increase T_{11} for all cases, because uniform crack surface loading showed positive T_{11} in Tables 3~6. In addition, cylinder thrust force will affect the results for the cases in Tables 8~11.

5. Conclusions

The T -stress solutions (T_{11} and T_{33}) for a semi-elliptical axial surface crack in a cylinder subjected to

mode-I non-uniform stresses on the crack surface are presented. Two cylinder geometries of $R_i/t = 5$ and 10 were considered. The T -stresses are presented along the crack front for a/t of 0.2, 0.4 and 0.5 and aspect ratios a/c of 0.2, 0.4, 0.6 and 1.0. Three stress distributions: uniform, linear and parabolic were applied to the crack face. Besides these solutions, concrete formulation of the superposition principle is given for the T_{33} -stress, which is known as an elastic parameter that describes the out-of-plane crack tip constraint effect. Then, the validity of the formulation was shown by applying our T -stress solutions to the problem of an axial semi-elliptical surface crack in a cylinder subjected to internal pressure, and checking that the principle of superposition holds for the problem.

Acknowledgement

Part of this work was supported by Japan Nuclear Energy Safety Organization. Their support is greatly appreciated.

List of Tables

Table 1 T_{11} , T_{33} stress solutions for quarter-elliptical corner crack in a finite thickness plate under remote uniform tension σ_0 ($a/t = 0.2$, $a/c = 0.4$, $W/c = 32$, $L/W = 1$, $\nu = 0.3$)

Table 2 Generated mesh size around crack

Table 3 T_{11} , T_{33} solutions for axial semi-elliptical surface crack in a cylinder subjected to mode-I non-uniform stress distribution ($R_i/t = 10$, $L/t = 20$, $a/t = 0.2, 0.4$ and 0.5 , $a/c = 0.2$ and 0.4 , $\nu = 0.3$)

Table 4 T_{11} , T_{33} solutions for axial semi-elliptical surface crack in a cylinder subjected to mode-I non-uniform stress distribution ($R_i/t = 10$, $L/t = 20$, $a/t = 0.2, 0.4$ and 0.5 , $a/c = 0.6$ and 1.0 , $\nu = 0.3$)

Table 5 T_{11} , T_{33} solutions for axial semi-elliptical surface crack in a cylinder subjected to mode-I non-uniform stress distribution ($R_i/t = 5$, $L/t = 20$, $a/t = 0.2, 0.4$ and 0.5 , $a/c = 0.2$ and 0.4 , $\nu = 0.3$)

Table 6 T_{11} , T_{33} solutions for axial semi-elliptical surface crack in a cylinder subjected to mode-I non-uniform stress distribution ($R_i/t = 5$, $L/t = 20$, $a/t = 0.2, 0.4$ and 0.5 , $a/c = 0.6$ and 1.0 , $\nu = 0.3$)

Table 7 Coefficients in Eq. (9): Quadratic approximation of the circumferential stress under internal pressure p

Table 8 Principle of superposition applied for T_{11} -stress solution for half-elliptical axial surface crack inside a pressurized cylinder ($R_i/t = 10$, $L/t = 20$, $t = 10$ mm, $\nu = 0.3$)

Table 9 Principle of superposition applied for T_{11} -stress solution for half-elliptical axial surface crack inside a pressurized cylinder ($R_i/t = 5$, $L/t = 20$, $t = 10$ mm, $\nu = 0.3$)

Table 10 Principle of superposition applied for T_{33} -stress solution for half-elliptical axial surface crack

inside a pressurized cylinder ($R_i/t = 10$, $L/t = 20$, $t = 10$ mm, $\nu = 0.3$)

Table 11 Principle of superposition applied for T_{33} -stress solution for half-elliptical axial surface crack

inside a pressurized cylinder ($R_i/t = 5$, $L/t = 20$, $t = 10$ mm, $\nu = 0.3$)

Table 1 T_{11} , T_{33} stress solutions for quarter-elliptical corner crack in a finite thickness plate under remote uniform tension σ_0 ($a/t = 0.2$, $a/c = 0.4$, $W/c = 32$, $L/W = 1$, $\nu = 0.3$)

	$\phi/(\pi/2)$	1/4	1/2	3/4
T_{11}	Current	-0.3676	-0.4318	-0.4449
	Qu [16]	-0.3788	-0.4390	-0.4625
	Difference %	-2.96	-1.64	-3.81
T_{33}	Current	-0.8025	-0.6426	-0.5933
	Qu [16]	-0.8321	-0.6621	-0.6078
	Difference %	-3.56	-2.80	-2.39

Table 2 Generated mesh size around crack

$R_i/t = 10$	$a/t = 0.2$				$a/t = 0.4$				$a/t = 0.5$			
a/c	0.2	0.4	0.6	1.0	0.2	0.4	0.6	1.0	0.2	0.4	0.6	1.0
$\Delta l/a$	0.03	0.01875	0.01875	0.03	0.03	0.01875	0.01875	0.03	0.03	0.025	0.025	0.03
$R_s/\Delta l$	5	8	8	5	5	8	8	5	5	6	6	5
$\Delta l_1/\Delta l$	2.00	2.00	2.00	1.98	2.00	2.00	2.00	2.00	2	2.136	2	2
$\Delta l_2/\Delta l$	4.47	7.87	7.87	3.72	3.73	6.56	6.56	3.73	3.72	3.45	2.92	2.79
$\Delta l_3/\Delta l$	4.53	7.39	7.39	4.53	3.25	5.49	5.51	3.25	3.72	3.06	3.11	2.48
$\Delta l_4/\Delta l$	11.05	9.52	9.52	8.83	5.61	7.20	7.20	4.49	7.06	8.48	8.48	7.06
L_{Box}/R_s	1.19	0.75	0.75	1.19	1.20	0.75	0.75	1.20	1.20	1.07	1	1.20
$\Delta c_d/\Delta l$	3.96	3.56	2.30	0.82	3.96	3.56	2.31	0.82	3.96	2.67	1.73	0.82
$\Delta c_e/\Delta l$	0.81	1.46	1.42	0.87	0.81	1.47	1.42	0.87	0.81	1.10	1.07	0.87
$R_i/t = 5$	$a/t = 0.2$				$a/t = 0.4$				$a/t = 0.5$			
a/c	0.2	0.4	0.6	1.0	0.2	0.4	0.6	1.0	0.2	0.4	0.6	1.0
$\Delta l/a$	0.0375	0.01875	0.025	0.01875	0.0375	0.01875	0.025	0.01875	0.0375	0.01875	0.025	0.01875
$R_s/\Delta l$	4	8	6	8	4	8	6	8	4	8	6	8
$\Delta l_1/\Delta l$	2	2	2	2	2	2	2	2	2	2	2	2
$\Delta l_2/\Delta l$	4.17	4.92	4	4.92	4.17	3.93	4	4.17	4.17	3.93	4	3.93
$\Delta l_3/\Delta l$	4.03	5.54	4.2	5.54	3.75	3.67	4	3.75	4.17	4.37	4	4.37
$\Delta l_4/\Delta l$	8.41	13.72	11.14	13.72	8.64	9.15	8.24	8.64	7.97	8.85	9.17	8.85
L_{Box}/R_s	1.5	0.75	1	0.75	1.5	0.75	1	0.75	1.5	0.75	1	0.75
$\Delta c_d/\Delta l$	3.82	3.56	1.73	1.31	3.82	3.56	1.73	1.31	3.82	3.56	1.73	1.31
$\Delta c_e/\Delta l$	0.78	1.47	1.07	1.40	0.78	1.47	1.07	1.40	0.78	1.47	1.07	1.40

Table 3 T_{11} , T_{33} solutions for axial semi-elliptical surface crack in a cylinder subjected to mode-Inon-uniform stress distribution ($R_i/t = 10$, $L/t = 20$, $a/t = 0.2, 0.4$ and 0.5 , $a/c = 0.2$ and 0.4 , $\nu = 0.3$)

a/c	i	$\phi/(\pi/2)$	$a/t = 0.2$		$a/t = 0.4$		$a/t = 0.5$	
			V_{11i}	V_{33i}	V_{11i}	V_{33i}	V_{11i}	V_{33i}
0.2	0	1/4	0.5185	-0.0710	0.4992	-0.1492	0.4984	-0.2145
		1/2	0.4761	0.0492	0.4560	-0.0020	0.4522	-0.0386
		3/4	0.4651	0.0812	0.4235	0.0293	0.3959	-0.0236
		1	0.4530	0.0865	0.3977	0.0278	0.3578	-0.0383
	1	1/4	0.0778	-0.0223	0.0719	-0.0501	0.0720	-0.0693
		1/2	0.1113	0.0037	0.1052	-0.0141	0.1045	-0.0258
		3/4	0.1382	0.0143	0.1228	-0.0045	0.1110	-0.0238
		1	0.1428	0.0163	0.1207	-0.0056	0.1017	-0.0309
	2	1/4	0.0182	-0.0064	0.0155	-0.0206	0.0156	-0.0290
		1/2	0.0405	0.0009	0.0380	-0.0083	0.0378	-0.0140
		3/4	0.0642	0.0030	0.0564	-0.0069	0.0495	-0.0168
		1	0.0705	0.0025	0.0583	-0.0091	0.0464	-0.0229
0.4	0	1/4	0.5749	-0.2203	0.5776	-0.3021	0.5833	-0.3683
		1/2	0.5114	-0.0705	0.5074	-0.1282	0.5084	-0.1707
		3/4	0.4875	-0.0149	0.4576	-0.0560	0.4284	-0.1031
		1	0.4524	-0.0089	0.4045	-0.0469	0.3558	-0.1013
	1	1/4	0.1183	-0.0679	0.1188	-0.0959	0.1206	-0.1169
		1/2	0.1372	-0.0381	0.1355	-0.0564	0.1349	-0.0725
		3/4	0.1537	-0.0268	0.1425	-0.0412	0.1304	-0.0579
		1	0.1432	-0.0287	0.1253	-0.0425	0.1050	-0.0618
	2	1/4	0.0390	-0.0080	0.0393	-0.0396	0.0402	-0.0496
		1/2	0.0568	0.0041	0.0560	-0.0286	0.0556	-0.0361
		3/4	0.0757	0.0072	0.0700	-0.0286	0.0634	-0.0373
		1	0.0712	0.0027	0.0619	-0.0338	0.0505	-0.0440

Table 4 T_{11} , T_{33} solutions for axial semi-elliptical surface crack in a cylinder subjected to mode-Inon-uniform stress distribution ($R_i/t = 10$, $L/t = 20$, $a/t = 0.2, 0.4$ and 0.5 , $a/c = 0.6$ and 1.0 , $\nu = 0.3$)

a/c	i	$\phi/(\pi/2)$	$a/t = 0.2$		$a/t = 0.4$		$a/t = 0.5$	
			V_{11i}	V_{33i}	V_{11i}	V_{33i}	V_{11i}	V_{33i}
0.6	0	1/4	0.5486	-0.2480	0.5476	-0.2974	0.5487	-0.3487
		1/2	0.5166	-0.1500	0.5135	-0.1953	0.5128	-0.2335
		3/4	0.4902	-0.1003	0.4674	-0.1284	0.4424	-0.1677
		1	0.4256	-0.1010	0.3883	-0.1286	0.3449	-0.1664
	1	1/4	0.1272	-0.0860	0.1265	-0.1042	0.1261	-0.1187
		1/2	0.1529	-0.0717	0.1512	-0.0850	0.1497	-0.0991
		3/4	0.1649	-0.0645	0.1564	-0.0751	0.1463	-0.0881
		1	0.1348	-0.0729	0.1213	-0.0823	0.1043	-0.0958
	2	1/4	0.0456	-0.0353	0.0452	-0.0444	0.0449	-0.0516
		1/2	0.0681	-0.0383	0.0672	-0.0444	0.0663	-0.0503
		3/4	0.0864	-0.0447	0.0821	-0.0500	0.0767	-0.0566
		1	0.0678	-0.0559	0.0610	-0.0608	0.0518	-0.0681
1.0	0	1/4	0.4284	-0.1864	0.4223	-0.2047	0.4168	-0.2295
		1/2	0.4491	-0.1814	0.4430	-0.2080	0.4381	-0.3824
		3/4	0.4560	-0.1943	0.4409	-0.2113	0.4647	-0.2648
		1	0.3331	-0.2359	0.3082	-0.2516	0.2806	-0.2702
	1	1/4	0.1044	-0.0758	0.1023	-0.0840	0.0999	-0.0913
		1/2	0.1504	-0.0949	0.1482	-0.1027	0.1139	-0.1089
		3/4	0.1768	-0.1155	0.1718	-0.1213	0.1444	-0.0858
		1	0.1045	-0.1479	0.0959	-0.1529	0.0858	-0.1599
	2	1/4	0.0371	-0.0323	0.0360	-0.0362	0.0347	-0.0396
		1/2	0.0731	-0.0540	0.0720	-0.0565	0.0361	-0.0345
		3/4	0.1046	-0.0804	0.1020	-0.0834	0.0571	-0.0768
		1	0.0539	-0.1114	0.0494	-0.1141	0.0441	-0.1180

Table 5 T_{11} , T_{33} solutions for axial semi-elliptical surface crack in a cylinder subjected to mode-Inon-uniform stress distribution ($R/t = 5$, $L/t = 20$, $a/t = 0.2, 0.4$ and 0.5 , $a/c = 0.2$ and 0.4 , $\nu = 0.3$)

a/c	i	$\phi/(\pi/2)$	$a/t = 0.2$		$a/t = 0.4$		$a/t = 0.5$	
			V_{11i}	V_{33i}	V_{11i}	V_{33i}	V_{11i}	V_{33i}
0.2	0	1/4	0.5131	-0.0744	0.4863	-0.1486	0.4838	-0.2013
		1/2	0.4693	0.0460	0.4366	-0.0072	0.4247	-0.0426
		3/4	0.4565	0.0771	0.3976	0.0161	0.3540	0.0409
		1	0.4436	0.0818	0.3688	0.0114	0.3086	0.0605
	1	1/4	0.0768	-0.0230	0.0693	-0.0491	0.0694	-0.0642
		1/2	0.1099	0.0032	0.1004	-0.0152	0.0972	-0.0262
		3/4	0.1359	0.0131	0.1150	-0.0088	0.0975	-0.0291
		1	0.14	0.0148	0.1114	-0.0111	0.0849	-0.0384
	2	1/4	0.0178	-0.0066	0.0144	-0.0201	0.0147	-0.0268
		1/2	0.0397	0.0003	0.0355	-0.0088	0.0342	-0.0138
		3/4	0.0629	0.0024	0.0521	-0.0089	0.0423	-0.0195
		1	0.0689	0.0018	0.0532	-0.0119	0.0373	-0.0267
0.4	0	1/4	0.5682	-0.2153	0.5562	-0.2910	0.5574	-0.3545
		1/2	0.5051	-0.0731	0.4854	-0.1222	0.4772	-0.1673
		3/4	0.4798	-0.0154	0.4346	-0.0607	0.3943	-0.1095
		1	0.4443	-0.0097	0.3816	-0.0534	0.3219	-0.1092
	1	1/4	0.1161	-0.0675	0.1128	-0.0937	0.1132	-0.1126
		1/2	0.1348	-0.0374	0.1285	-0.0566	0.1252	-0.0710
		3/4	0.1504	-0.0268	0.1347	-0.0426	0.1190	-0.0598
		1	0.1397	-0.0292	0.1172	-0.0446	0.0935	-0.0647
	2	1/4	0.0382	-0.0256	0.0367	-0.0383	0.0368	-0.0473
		1/2	0.0559	-0.0194	0.0530	-0.0284	0.0511	-0.0359
		3/4	0.0745	-0.0214	0.0664	-0.0294	0.0578	-0.0381
		1	0.0698	-0.0269	0.0581	-0.0347	0.0447	-0.0453

Table 6 T_{11} , T_{33} solutions for axial semi-elliptical surface crack in a cylinder subjected to mode-Inon-uniform stress distribution ($R_i/t = 5$, $L/t = 20$, $a/t = 0.2, 0.4$ and 0.5 , $a/c = 0.6$ and 1.0 , $\nu = 0.3$)

a/c	i	$\phi/(\pi/2)$	$a/t = 0.2$		$a/t = 0.4$		$a/t = 0.5$	
			V_{11i}	V_{33i}	V_{11i}	V_{33i}	V_{11i}	V_{33i}
0.6	0	1/4	0.5420	-0.2391	0.5294	-0.2930	0.5244	-0.3299
		1/2	0.5108	-0.1444	0.4945	-0.1883	0.4852	-0.2242
		3/4	0.4837	-0.0982	0.4484	-0.1303	0.4150	-0.1680
		1	0.4177	-0.1013	0.3684	-0.1305	0.3185	-0.1681
	1	1/4	0.1248	-0.0841	0.1209	-0.1007	0.1189	-0.1149
		1/2	0.1505	-0.0693	0.1452	-0.0839	0.1412	-0.0963
		3/4	0.1621	-0.0640	0.1502	-0.0748	0.1376	-0.0878
		1	0.1311	-0.0727	0.1143	-0.0827	0.0955	-0.0966
	2	1/4	0.0447	-0.0344	0.0427	-0.0427	0.0416	-0.0493
		1/2	0.0672	-0.0370	0.0645	-0.0439	0.0622	-0.0492
		3/4	0.0853	-0.0442	0.0792	-0.0500	0.0723	-0.0565
		1	0.0661	-0.0560	0.0575	-0.0612	0.0473	-0.0684
1.0	0	1/4	0.4238	-0.1763	0.4109	-0.1988	0.4021	-0.2172
		1/2	0.4439	-0.1774	0.4299	-0.1981	0.4208	-0.2238
		3/4	0.4507	-0.1874	0.4279	-0.2057	0.4068	-0.2308
		1	0.3323	-0.2340	0.3005	-0.2477	0.2689	-0.2675
	1	1/4	0.1031	-0.0746	0.0989	-0.0818	0.0957	-0.0880
		1/2	0.1488	-0.0943	0.1441	-0.1018	0.1404	-0.1091
		3/4	0.1752	-0.1152	0.1677	-0.1203	0.1599	-0.1282
		1	0.1054	-0.1466	0.0947	-0.1519	0.0832	-0.1590
	2	1/4	0.0366	-0.0315	0.0345	-0.0349	0.0328	-0.0385
		1/2	0.0725	-0.0532	0.0702	-0.0570	0.0681	-0.0607
		3/4	0.1039	-0.0802	0.1002	-0.0831	0.0960	-0.0873
		1	0.0550	-0.1108	0.0496	-0.1137	0.0435	-0.1174

Table 7 Coefficients in Eq. (9): Quadratic approximation of the circumferential stress under internal

pressure p

R_i/t	a/t	σ_0/p	σ_1/p	σ_2/p
10	0.2	10.524	-0.230	0.006
	0.4	10.523	-0.458	0.024
	0.5	10.523	-0.571	0.036
5	0.2	5.545	-0.260	0.013
	0.4	5.544	-0.512	0.047
	0.5	5.542	-0.633	0.068

Table 8 Principle of superposition applied for T_{11} -stress solution for half-elliptical axial surface crack inside a pressurized cylinder ($R_i/t = 10, L/t = 20, t = 10$ mm, $\nu = 0.3$)

a/c	ϕ' ($\pi/2$)	$a/t = 0.2$			$a/t = 0.4$			$a/t = 0.5$		
		T_{11}/p	$T_{11 \text{ sup}}/p$	Δ %	T_{11}/p	$T_{11 \text{ sup}}/p$	Δ %	T_{11}/p	$T_{11 \text{ sup}}/p$	Δ %
0.2	1/4	-5.7358	-5.7378	-0.03	-5.7992	-5.8018	-0.05	-5.7406	-5.7431	-0.04
	1/2	-6.1857	-6.1872	-0.02	-6.1197	-6.1210	-0.02	-6.0254	-6.0270	-0.03
	3/4	-6.2387	-6.2404	-0.03	-6.3101	-6.3113	-0.02	-6.4196	-6.4204	-0.01
	1	-6.3388	-6.3410	-0.04	-6.5199	-6.5237	-0.06	-6.7388	-6.7433	-0.07
0.4	1/4	-4.8797	-4.8854	-0.12	-4.7635	-4.7654	-0.04	-4.6436	-4.6458	-0.05
	1/2	-5.7345	-5.7380	-0.06	-5.5240	-5.5250	-0.02	-5.3903	-5.3908	-0.01
	3/4	-5.9910	-5.9932	-0.04	-5.9483	-5.9495	-0.02	-6.0791	-6.0797	-0.01
	1	-6.3456	-6.3476	-0.03	-6.4498	-6.4535	-0.06	-6.7616	-6.7666	-0.07
0.6	1/4	-4.9873	-4.9870	0.01	-4.9122	-4.9132	-0.02	-4.8586	-4.8602	-0.03
	1/2	-5.5804	-5.5809	-0.01	-5.3802	-5.3809	-0.01	-5.2747	-5.2754	-0.01
	3/4	-5.9410	-5.9422	-0.02	-5.8317	-5.8337	-0.03	-5.9235	-5.9247	-0.02
	1	-6.6261	-6.6275	-0.02	-6.6183	-6.6222	-0.06	-6.8753	-6.8802	-0.07
1	1/4	-6.0862	-6.0857	0.01	-6.0740	-6.0748	-0.01	-6.0934	-6.0947	-0.02
	1/2	-6.0919	-6.0924	-0.01	-5.9582	-5.9591	-0.02	-5.9101	-5.9107	-0.01
	3/4	-6.2321	-6.2343	-0.03	-6.0638	-6.0658	-0.03	-6.0795	-6.0814	-0.03
	1	-7.5914	-7.5944	-0.04	-7.4499	-7.4544	-0.06	-7.5421	-7.5475	-0.07

Table 9 Principle of superposition applied for T_{11} -stress solution for half-elliptical axial surface crack inside a pressurized cylinder ($R_i/t = 5$, $L/t = 20$, $t = 10$ mm, $\nu = 0.3$)

a/c	$\phi/(\pi/2)$	$a/t = 0.2$			$a/t = 0.4$			$a/t = 0.5$		
		T_{11}/p	$T_{11 \text{ sup}}/p$	Δ %	T_{11}/p	$T_{11 \text{ sup}}/p$	Δ %	T_{11}/p	$T_{11 \text{ sup}}/p$	Δ %
0.2	1/4	-3.3513	-3.3533	-0.06	-3.3466	-3.3494	-0.08	-3.2868	-3.2905	-0.11
	1/2	-3.5828	-3.5841	-0.04	-3.4661	-3.4685	-0.07	-3.3915	-3.3937	-0.07
	3/4	-3.5836	-3.5849	-0.04	-3.5230	-3.5246	-0.05	-3.5772	-3.5788	-0.05
	1	-3.6249	-3.6270	-0.06	-3.6195	-3.6218	-0.06	-3.7476	-3.7501	-0.07
0.4	1/4	-2.7932	-2.7933	-0.002	-2.7443	-2.7456	-0.05	-2.6819	-2.6845	-0.10
	1/2	-3.3100	-3.3107	-0.02	-3.1455	-3.1460	-0.02	-3.0604	-3.0615	-0.04
	3/4	-3.4421	-3.4439	-0.05	-3.3165	-3.3174	-0.03	-3.3588	-3.3593	-0.01
	1	-3.6199	-3.6226	-0.07	-3.5493	-3.5538	-0.13	-3.6767	-3.6813	-0.13
0.6	1/4	-2.7655	-2.7648	0.03	-2.7395	-2.7410	-0.06	-2.7200	-2.7220	-0.07
	1/2	-3.1783	-3.1784	-0.003	-3.0189	-3.0199	-0.03	-2.9518	-2.9526	-0.03
	3/4	-3.3997	-3.4011	-0.04	-3.2288	-3.2305	-0.05	-3.2390	-3.2399	-0.03
	1	-3.7661	-3.7683	-0.06	-3.6216	-3.6253	-0.10	-3.6977	-3.7014	-0.10
1	1/4	-3.2576	-3.2561	0.05	-3.2450	-3.2443	0.02	-3.2505	-3.2517	-0.04
	1/2	-3.3554	-3.3549	0.01	-3.2218	-3.2219	-0.003	-3.1707	-3.1713	-0.02
	3/4	-3.5171	-3.5187	-0.05	-3.3002	-3.3024	-0.07	-3.2551	-3.2565	-0.04
	1	-4.2310	-4.2350	-0.09	-3.9862	-3.9923	-0.15	-3.9632	-3.9687	-0.14

Table 10 Principle of superposition applied for T_{33} -stress solution for half-elliptical axial surface crack inside a pressurized cylinder ($R_i/t = 10$, $L/t = 20$, $t = 10$ mm, $\nu = 0.3$)

a/c	$\phi/(\pi/2)$	$a/t = 0.2$			$a/t = 0.4$			$a/t = 0.5$		
		T_{33}/p	$T_{33 \text{ sup}}/p$	Δ %	T_{33}/p	$T_{33 \text{ sup}}/p$	Δ %	T_{33}/p	$T_{33 \text{ sup}}/p$	Δ %
0.2	1/4	-7.1731	-7.1768	-0.05	-7.9696	-7.9148	0.69	-8.5900	-8.5529	0.43
	1/2	-5.7345	-5.7337	0.01	-6.1653	-6.1684	-0.05	-6.4928	-6.4979	-0.08
	3/4	-5.3384	-5.3440	-0.11	-5.7613	-5.7660	-0.08	-6.2562	-6.2551	0.02
	1	-5.2718	-5.2737	-0.04	-5.7579	-5.7582	-0.01	-6.3874	-6.3790	0.13
0.4	1/4	-8.9791	-9.0059	-0.30	-9.7289	-9.7465	-0.18	-10.3488	-10.3757	-0.26
	1/2	-7.0709	-7.0675	0.05	-7.4867	-7.5449	-0.78	-7.9442	-7.9229	0.27
	3/4	-6.3650	-6.3620	0.05	-6.6677	-6.6597	0.12	-7.0760	-7.0825	-0.09
	1	-6.2705	-6.2669	0.06	-6.5252	-6.5288	-0.05	-7.0116	-7.0253	-0.20
0.6	1/4	-9.4526	-9.4706	-0.19	-9.8967	-9.8544	0.43	-10.3348	-10.3219	0.12
	1/2	-7.9408	-8.0038	-0.79	-8.2965	-8.3255	-0.35	-8.6803	-8.6474	0.38
	3/4	-7.2608	-7.2776	-0.23	-7.4366	-7.4252	0.15	-7.7682	-7.7613	0.09
	1	-7.2388	-7.2262	0.17	-7.3642	-7.3709	-0.09	-7.6843	-7.6913	-0.09
1	1/4	-8.9380	-8.9861	-0.54	-9.0960	-9.0340	0.68	-9.1970	-9.2206	-0.26
	1/2	-8.5006	-8.5268	-0.31	-8.5732	-8.6134	-0.47	-8.7131	-8.7000	0.15
	3/4	-8.2782	-8.3246	-0.56	-8.2847	-8.3301	-0.55	-8.4626	-8.4685	-0.07
	1	-8.6366	-8.6287	0.09	-8.6272	-8.6334	-0.07	-8.7475	-8.7486	-0.01

Table 11 Principle of superposition applied for T_{33} -stress solution for half-elliptical axial surface crack inside a pressurized cylinder ($R_i/t = 10$, $L/t = 20$, $t = 10$ mm, $\nu = 0.3$)

a/c	ϕ' ($\pi/2$)	$a/t = 0.2$			$a/t = 0.4$			$a/t = 0.5$		
		T_{33}/p	$T_{33 \text{ sup}}/p$	Δ %	T_{33}/p	$T_{33 \text{ sup}}/p$	Δ %	T_{33}/p	$T_{33 \text{ sup}}/p$	Δ %
0.2	1/4	-3.8277	-3.8457	-0.47	-4.1707	-4.1653	0.13	-4.3968	-4.4069	-0.23
	1/2	-2.9939	-2.9980	-0.14	-3.1772	-3.1814	-0.13	-3.3191	-3.3198	-0.02
	3/4	-2.7722	-2.7708	0.05	-2.9768	-2.9770	-0.008	-3.2207	-3.2221	-0.04
	1	-2.7295	-2.7292	0.01	-2.9786	-2.9793	-0.02	-3.2990	-3.2989	0.002
0.4	1/4	-4.8907	-4.8804	0.21	-5.1777	-5.1703	0.14	-5.4005	-5.4507	-0.93
	1/2	-3.7052	-3.7299	-0.66	-3.8590	-3.8641	-0.13	-4.0599	-4.0422	0.34
	3/4	-3.2919	-3.2890	-0.09	-3.3962	-3.3978	-0.05	-3.5921	-3.5932	-0.03
	1	-3.2296	-3.2251	-0.14	-3.3277	-3.3223	0.16	-3.5546	-3.5537	0.03
0.6	1/4	-5.2202	-5.1836	0.70	-5.2997	-5.2254	-0.67	-5.4894	-5.4618	0.50
	1/2	-4.2064	-4.2217	-0.37	-4.2654	-4.3010	-0.83	-4.4194	-4.4160	0.08
	3/4	-3.7625	-3.7629	-0.01	-3.7837	-3.7858	-0.06	-3.9135	-3.9159	-0.06
	1	-3.7254	-3.7223	0.08	-3.7295	-3.7313	-0.05	-3.8532	-3.8616	-0.22
1	1/4	-5.0083	-4.9972	0.22	-4.9726	-4.9648	0.16	-5.0126	-4.9882	0.49
	1/2	-4.6095	-4.5915	0.39	-4.5015	-4.5013	0.005	-4.5197	-4.5434	-0.52
	3/4	-4.3364	-4.3127	0.55	-4.2459	-4.2323	0.32	-4.2810	-4.2820	-0.02
	1	-4.4376	-4.4398	-0.05	-4.3394	-4.3482	-0.20	-4.3840	-4.3759	0.18

List of Figures

Fig. 1 Three-dimensional coordinate system for the region along the crack front

Fig. 2 Axial surface crack inside a cylinder

Fig. 3 Principle of superposition

Fig. 4 Quarter-elliptical corner crack in a finite thickness plate under remote uniform tension σ_0 : structure and finite element model

Fig. 5 Mesh size around crack

Fig. 6 Typical finite element meshes ($a/t = 0.2$, $a/c = 0.4$, $R_i/t = 10$, $L/t = 20$, $t = 10$ mm, $\nu = 0.3$)

References

- [1] Shih CF, German MD. Requirements for a one parameter characterization of crack tip fields by the HRR singularity. *International Journal of Fracture*. 1981;17(1):27-43.
- [2] Larsson SG, Carlsson AJ. Influence of non-singular stress terms and specimen geometry on small-scale yielding at crack tips in elastic-plastic materials. *Journal of the Mechanics and Physics of Solids*. 1973;21(4):263-277.
- [3] Williams ML. On the stress distribution at the base of a stationary crack. *Journal of applied mechanics*. 1957;24:111-114.
- [4] Rice JR. Limitations to the small scale yielding approximation for crack tip plasticity. *Journal of the Mechanics and Physics of Solids*. 1974;22(1):17-26.
- [5] Bilby BA, Cardew GE, Goldthorpe MR, Howard IC. A finite element investigation of the effect of specimen geometry on the fields of stress and strain at the tips of stationary cracks. . *Size Effects in Fracture*. London: Mechanical Engineering Publications Limited, 1986. p. 37-46.
- [6] Al-Ani AM, Hancock JW. J-Dominance of short cracks in tension and bending. *Journal of the Mechanics and Physics of Solids*. 1991;39(1):23-43.
- [7] Betegon C, Hancock JW. Two-parameter characterization of elastic-plastic crack-tip fields. *Journal of Applied Mechanics* 1991;58(1):104-110.
- [8] Du ZZ, Hancock JW. The effect of non-singular stresses on crack-tip constraint. *Journal of the Mechanics and Physics of Solids*. 1991;39(4):555-567.
- [9] O'Dowd NP, Shih CF. Family of crack-tip fields characterized by a triaxiality parameter--I. Structure of fields. *Journal of the Mechanics and Physics of Solids*. 1991;39(8):989-1015.
- [10] Kirk MT, Dodds RH, Anderson TL. An Approximate Technique for Predicting Size Effects on Cleavage Fracture Toughness (J_c) Using the Elastic T Stress In: Landes JD, McCabe DE, Boulet JAM, editors. STP 1207, *Fracture Mechanics: Twenty-Fourth Volume* Philadelphia: American Society for Testing and Materials, 1994. p. 62-86.
- [11] Kong XM, Schluter N, Dahl W. Effect of triaxial stress on mixed-mode fracture. *Engineering Fracture Mechanics*. 1995;52(2):379-385.
- [12] Gao H. Variation of elastic T-stresses along slightly wavy 3D crack fronts. *International Journal of Fracture*. 1992;58(3):241-257.
- [13] Nakamura T, Parks DM. Determination of elastic T-stress along three-dimensional crack fronts using an interaction integral. *International journal of solids and structures*. 1992;29(13):1597-1611.
- [14] Wang X. Elastic T-stress solutions for semi-elliptical surface cracks in finite thickness plates. *Engineering Fracture Mechanics*. 2003;70(6):731-756.
- [15] Wang X, Bell R. Elastic T-stress solutions for semi-elliptical surface cracks in finite thickness plates subject to non-uniform stress distributions. *Engineering Fracture Mechanics*.

2004;71(9-10):1477-1496.

- [16] Qu J, Wang X. Solutions of T-stresses for quarter-elliptical corner cracks in finite thickness plates subject to tension and bending. *International Journal of Pressure Vessels and Piping*. 2006;83(8):593-606.
- [17] Gullerud A, Koppenhoefer K, Roy Y, RoyChowdhury S, Walters M, Bichon B, Cochran K, Dodds Jr R. WARP3D Release 15 Manual. Civil Engineering, Report No UIUCENG-95-2012, University of Illinois at Urbana-Champaign. 2004.
- [18] Zhao J, Guo W, She C. The in-plane and out-of-plane stress constraint factors and $K - T - T_z$ description of stress field near the border of a semi-elliptical surface crack. *International Journal of Fatigue*. 2007;29(3):435-443.
- [19] Lewis T, Wang X. The T-stress solutions for through-wall circumferential cracks in cylinders subjected to general loading conditions. *Engineering Fracture Mechanics*. 2008;75(10):3206-3225.
- [20] Barsoum RS. Triangular quarter-point elements as elastic and perfectly-plastic crack tip elements. *International Journal for Numerical Methods in Engineering*. 1977;11(1):85-98.
- [21] Timoshenko S, Goodier J. *Theory of Elasticity*, Third edition. New York: McGraw-Hill, 1990.

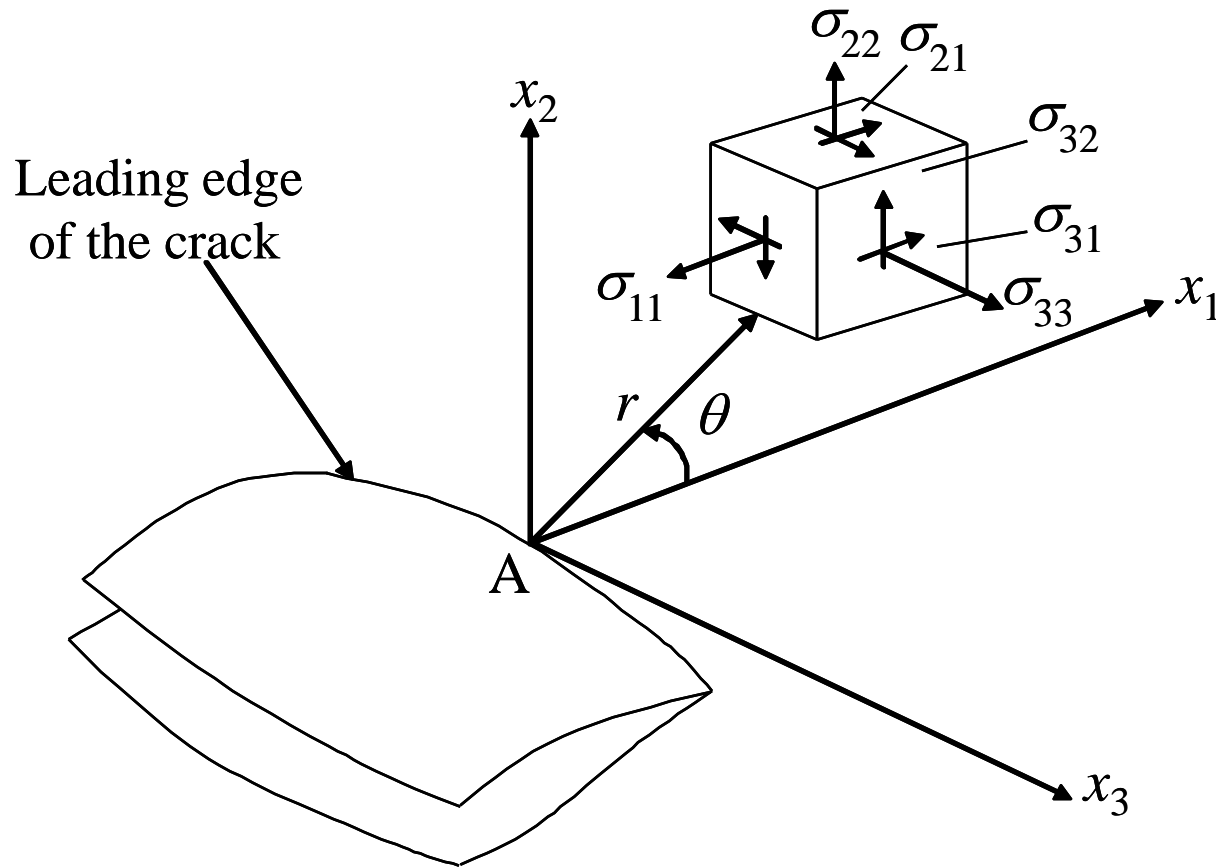


Fig. 1 Three-dimensional coordinate system for the region along the crack front

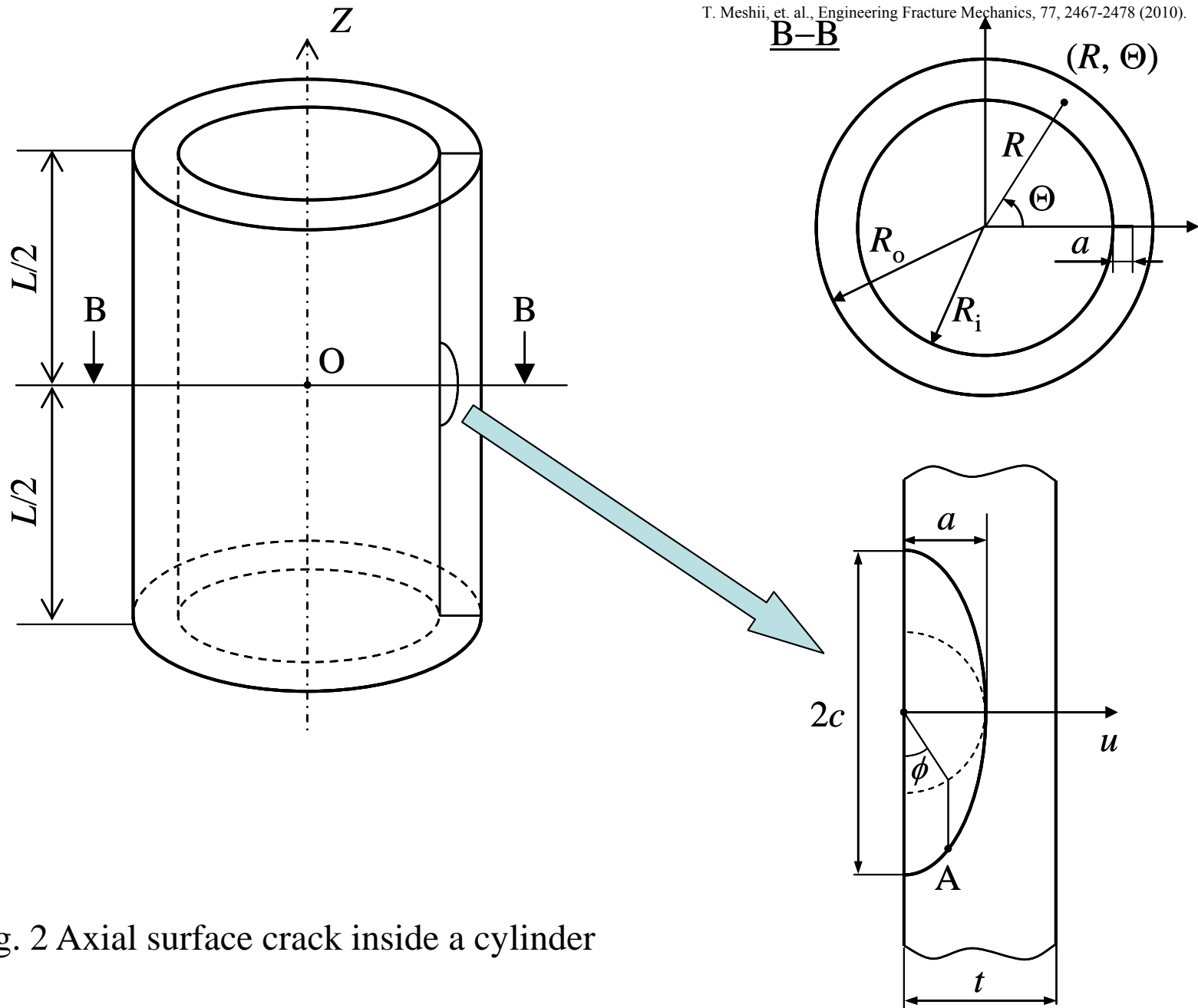


Fig. 2 Axial surface crack inside a cylinder

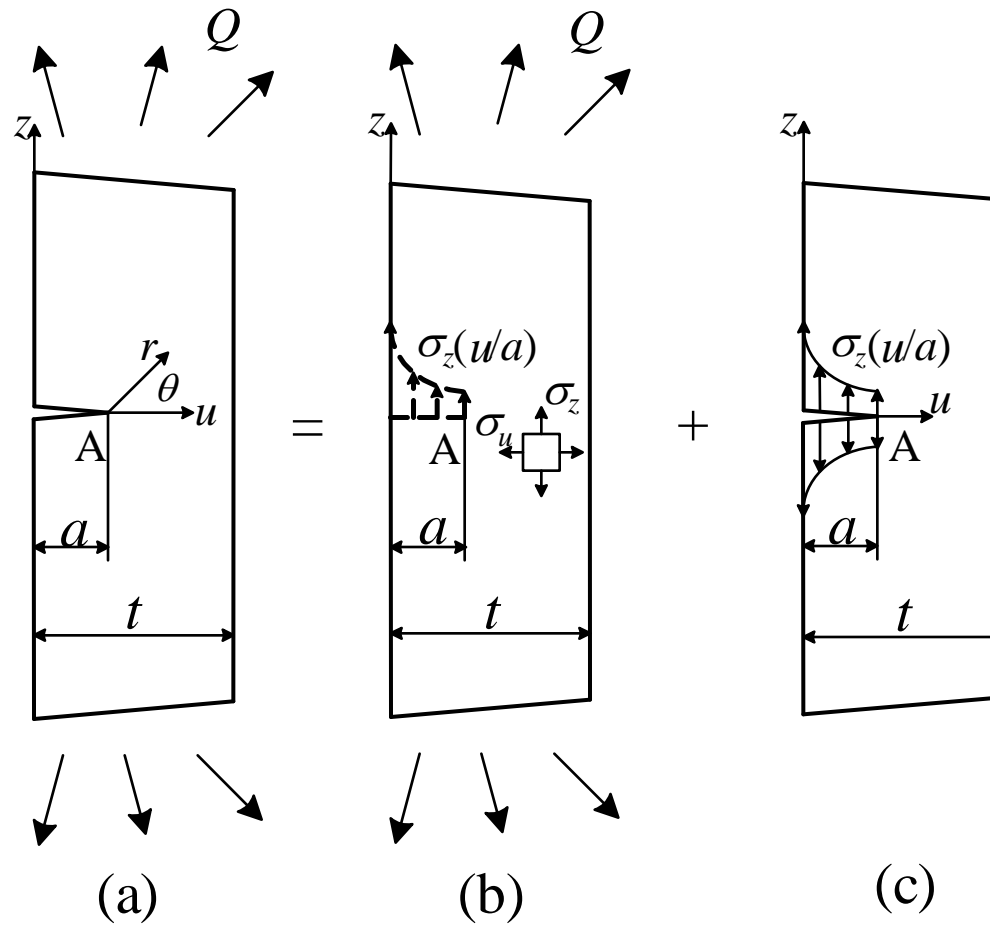


Fig. 3 Principle of superposition

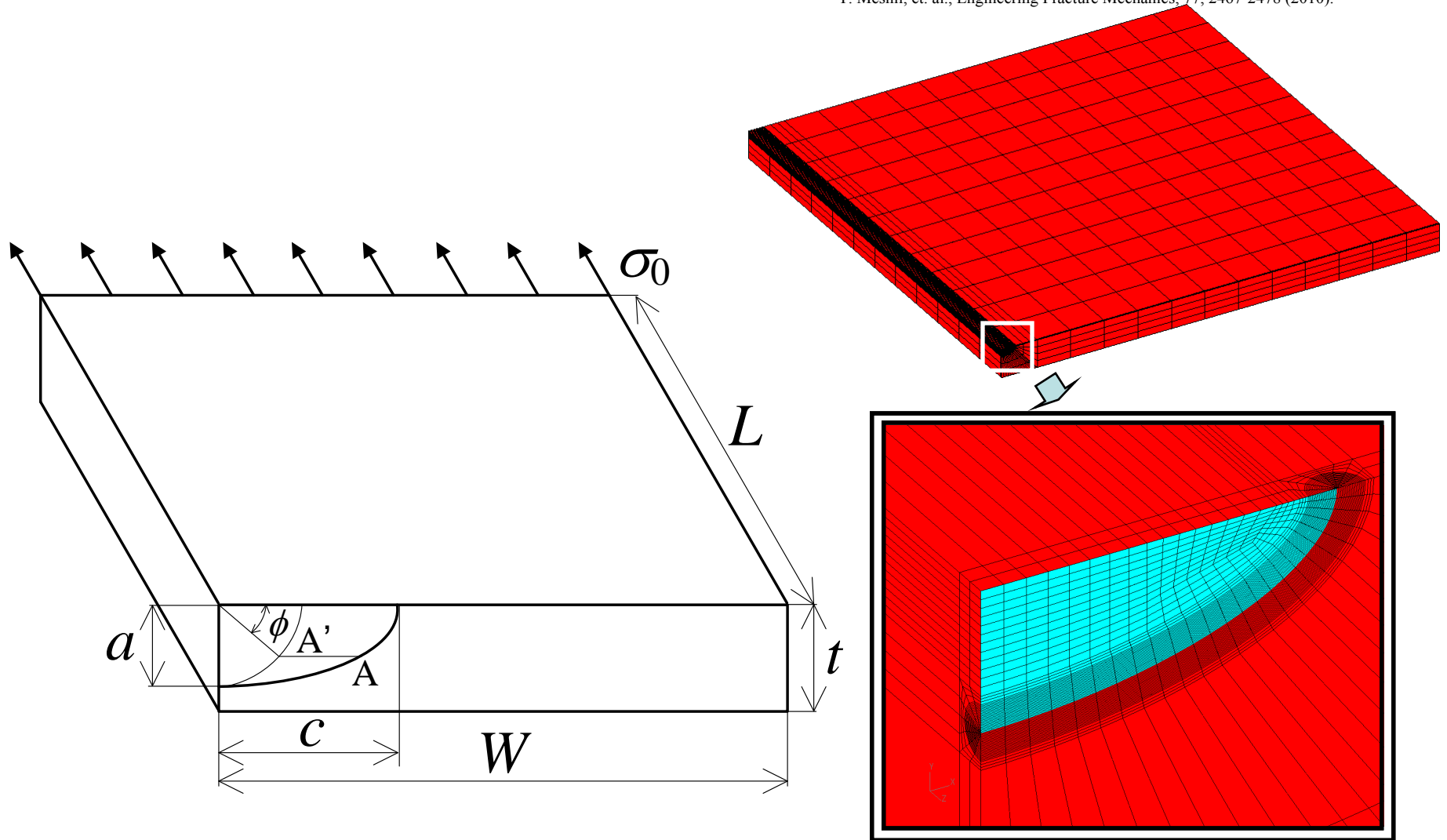


Fig. 4 Quarter-elliptical corner crack in a finite thickness plate under remote uniform tension σ_0 : structure and finite element model

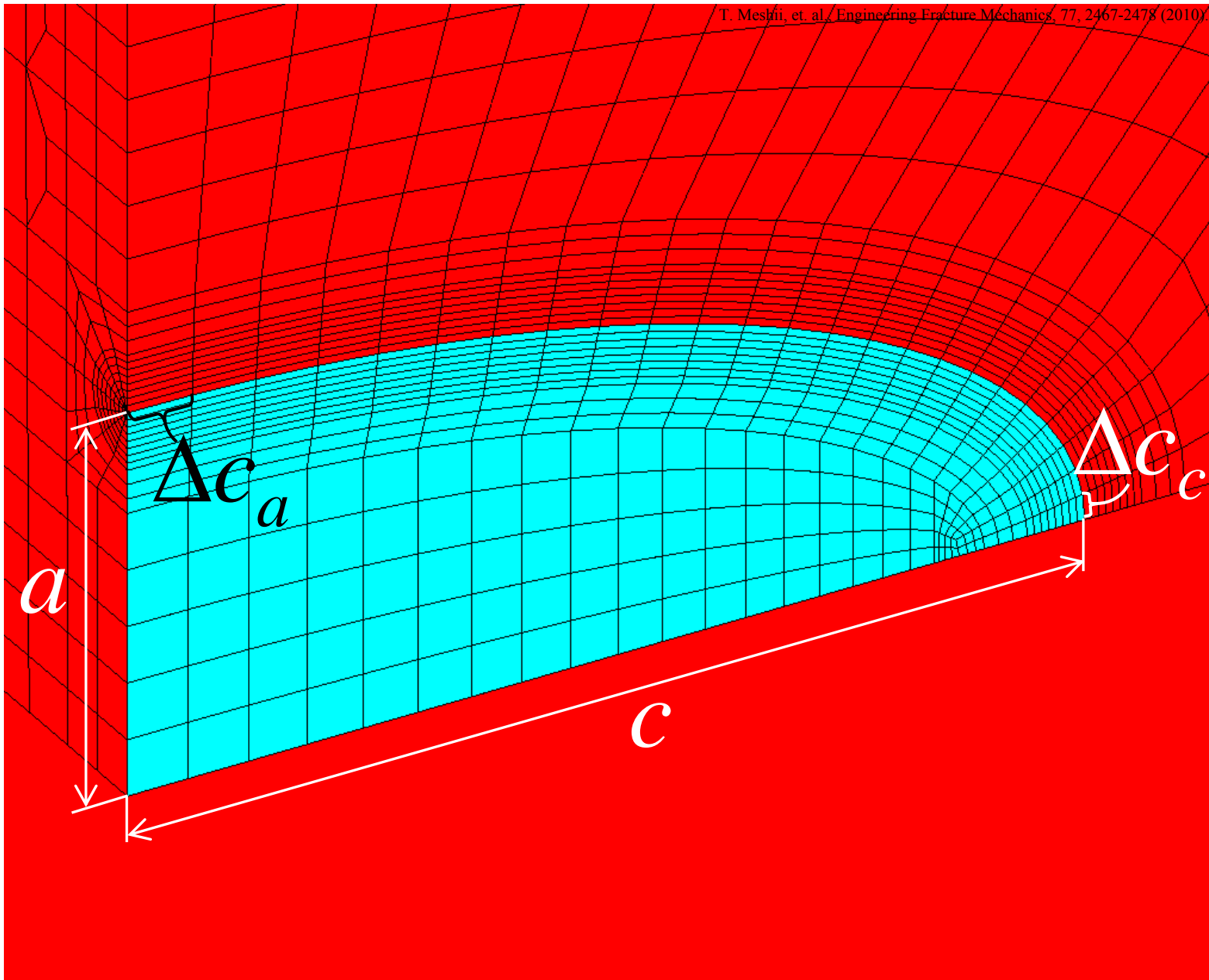


Fig. 5 (a) Mesh size around crack front

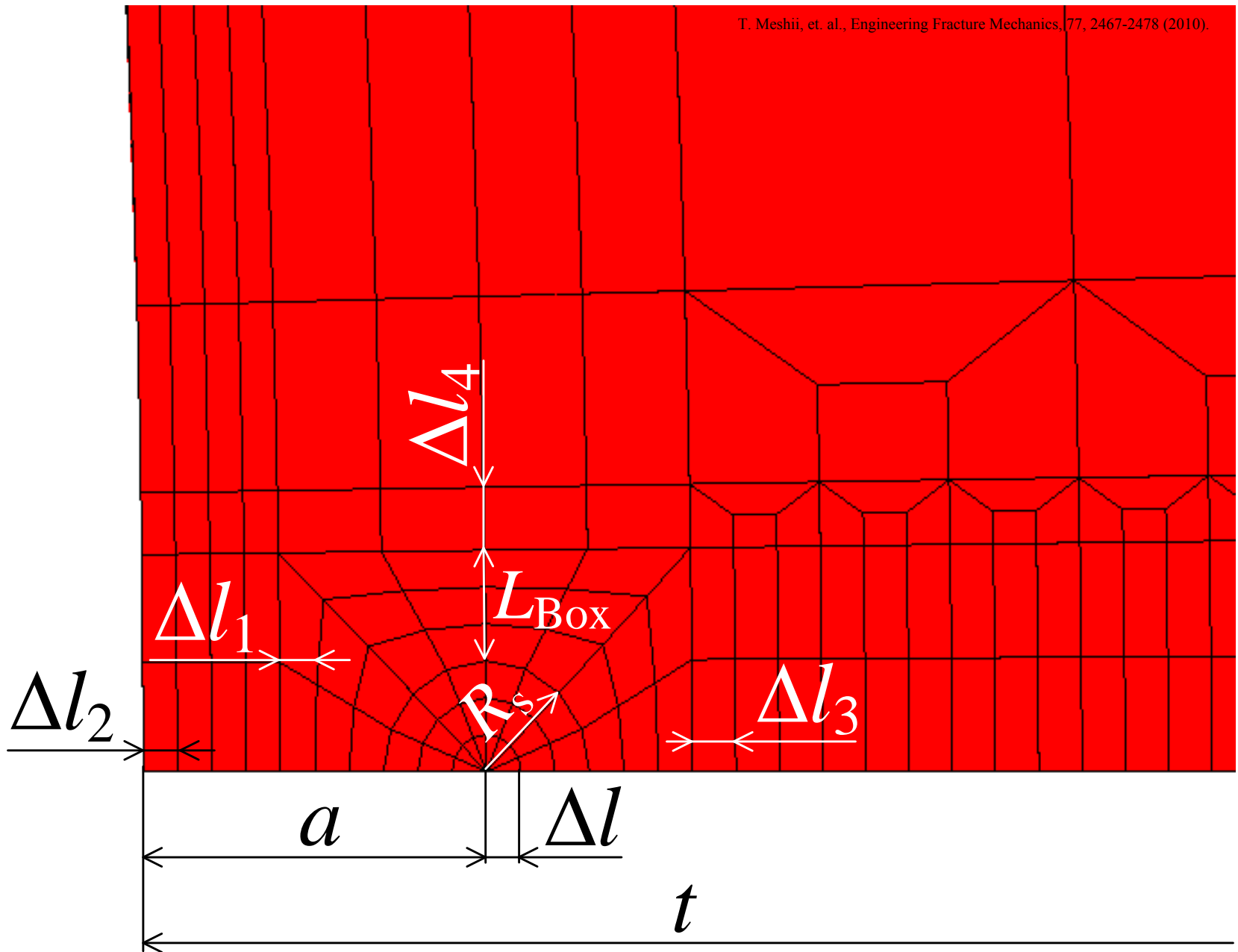


Fig. 5 (b) Mesh size around crack tip

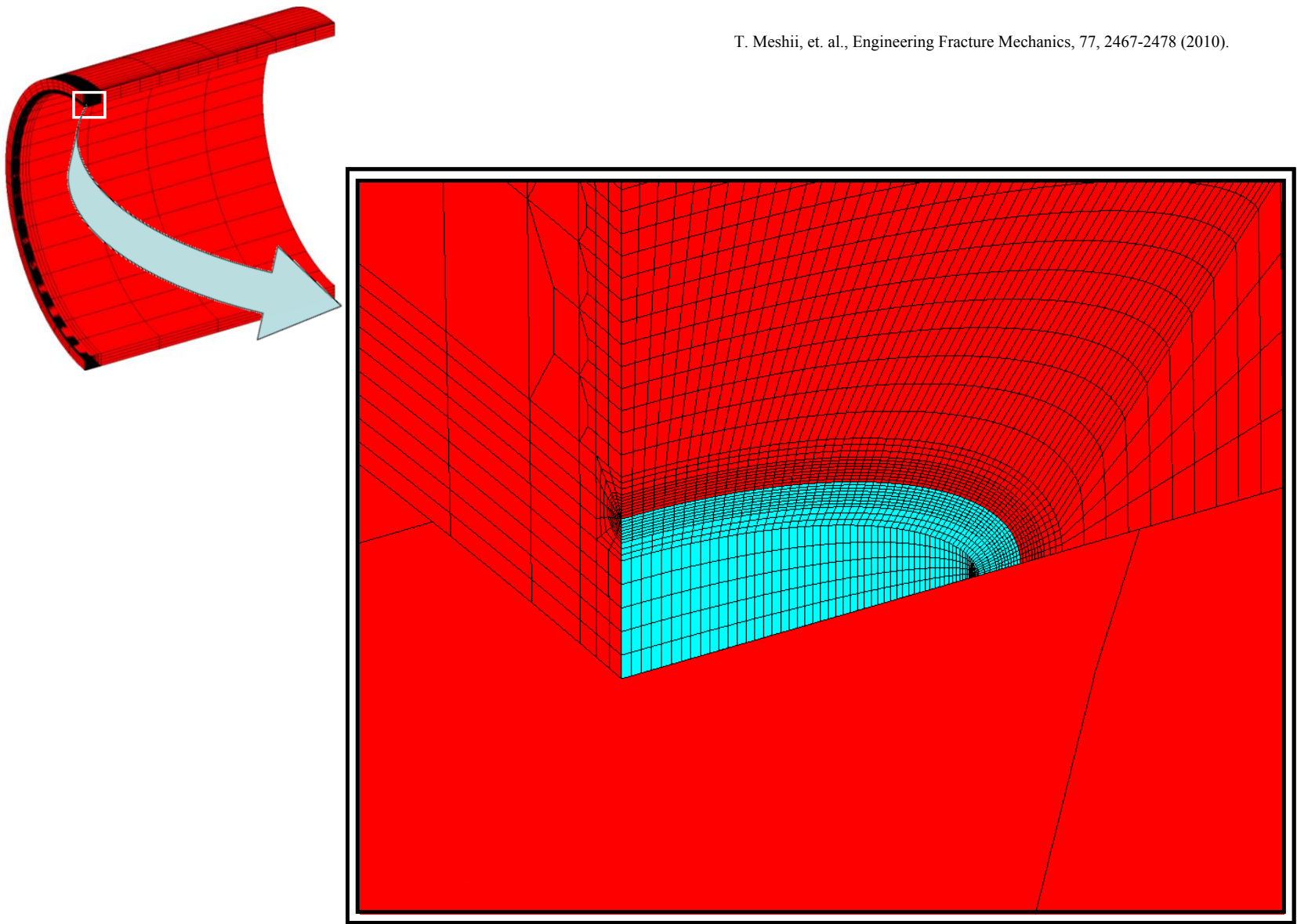


Fig. 6 Typical finite element meshes ($a/t = 0.2$, $a/c = 0.4$, $R_1/t = 10$, $L/t = 20$, $t = 10$ mm, $\nu = 0.3$)